Eddy–Zonal Flow Feedback in the Northern Hemisphere Winter

DAVID J. LORENZ AND DENNIS L. HARTMANN

Department of Atmospheric Sciences, University of Washington, Seattle, Washington

(Manuscript received 18 April 2002, in final form 16 September 2002)

ABSTRACT

The variability of the zonal-mean zonal wind in the Northern Hemisphere winter (December–March) is studied using EOF analysis and momentum budget diagnostics of NCEP–NCAR reanalysis data (1976–2001). The leading EOF of the zonal-mean zonal wind is well separated from the remaining EOFs and represents the north–south movement of the midlatitude westerlies. Analysis of the momentum budget shows that a positive feedback between the zonal-mean wind anomalies and the eddy momentum fluxes selects the leading EOF of midlatitude variability. Like the Southern Hemisphere, the baroclinic eddies reinforce the zonal wind anomalies while external Rossby waves damp the wind anomalies. In the Northern Hemisphere, the quasi-stationary eddies also reinforce the zonal wind anomalies, but the baroclinic eddies are most important for the positive eddy–zonal flow feedback. The observations support the following feedback mechanisms. 1) Above-normal baroclinic wave activity is generated in the region of enhanced westerlies. This leads to wave propagation out of the westerlies that is associated with reinforcing eddy momentum fluxes. 2) The westerly jet is a waveguide for external Rossby waves that tend to propagate into the jet and remove momentum from it. 3) The quasi-stationary waves respond to a refractive index anomaly in the high latitudes below the tropopause. During the high (low) index this anomaly is negative (positive) leading to an acceleration (deceleration) of the zonal wind in the high latitudes.

1. Introduction

The annular mode is the leading pattern of month-to-month variability of sea level pressure in both the Northern and the Southern Hemispheres (Thompson and Wallace 2000). This annular pattern is remarkably zonally symmetric in both hemispheres despite the strong longitudinal asymmetries in the Northern Hemisphere (NH) climate compared to the Southern Hemisphere (SH). The zonal-mean zonal wind anomalies associated with the annular mode and the effect of the eddies on the wind anomalies both in observations and in general circulation models has been the subject of much previous work (Kidson 1988; Karoly 1990; Robinson 1991, 1994, 1996; James and James 1992; Yu and Hartmann 1993; Hartmann 1995; Feldstein and Lee 1996, 1998; Lee and Feldstein 1996; Akahori and Yoden 1997; Hartmann and Lo 1998; Limpasuvan and Hartmann 1999, 2000; Hartmann et. al. 2000; Lorenz and Hartmann 2001, hereafter LH01). Most of these studies argue that a positive feedback between the zonal-mean wind anomalies and the eddies is important for maintaining the wind anomalies associated with the annular modes. Recently, LH01 provided a quantitative estimate of the effect of an eddy–zonal flow feedback on the variability of the zonal-mean flow in the SH. LH01 argued that a positive feedback accounts for the greater persistence of EOF1 zonal wind variability compared to EOF2 variability and that the positive feedback is important for the selection of the leading pattern of zonal-mean month-to-month variability. LH01 also found that high-frequency, or synoptic, eddies account for the positive feedback in the SH, which is consistent with previous studies (Karoly 1990; Robinson 1991; Yu and Hartmann 1993; Feldstein and Lee 1998; Hartmann and Lo 1998; Limpasuvan and Hartmann 2000). In the NH, recent work (DeWeaver and Nigam 2000a,b; Limpasuvan and Hartmann 1999, 2000; Kimoto et al. 2001) has also suggested that a feedback between the eddies and the zonal-mean flow is important for the selection of the leading pattern of variability. These papers also imply that, in contrast to the SH, the quasi-stationary waves rather than the synoptic (i.e., high frequency) waves are the dominant contributors to the eddy–zonal flow feedback.

In this paper we extend the SH study of LH01 to the NH winter. We show that the strength of the positive eddy–zonal flow feedback accounts for the larger persistence and variance of EOF1 compared to EOF2. Our diagnosis also shows that the synoptic (i.e., high frequency) eddies contribute more to the positive feedback than the quasi-stationary eddies. In addition, we describe the dynamics of the eddy response to the zonal wind anomalies. This paper begins with the data and analysis section followed by a discussion of the time-

Corresponding author address: Mr. David J. Lorenz, Department of Atmospheric Sciences, University of Washington, Box 351640, Seattle, WA 98195.
E-mail: djlorenz@atmos.washington.edu

mean zonal-mean flow and the leading EOF's (section 3). Section 4 presents the time series analysis and the simple model that provides a quantitative estimate of the effect of the eddy–zonal wind feedback on the zonal-mean variability. In section 5 we compare the contribution of the synoptic and quasi-stationary waves to the positive eddy–zonal flow feedback and in section 6 we describe the dynamics of the positive feedback. We end with a summary and discussion.

2. Data and analysis

a. Data

For this study, we used the National Centers for Environmental Prediction–National Center for Atmospheric Research (NCEP–NCAR) reanalysis four-times-daily wind, temperature, and geopotential height on constant pressure levels (Kalnay et al. 1996). We used data for Northern Hemisphere winter (December–March; DJFM) from December 1976 to March 2001 on a 2.5° × 2.5° latitude–longitude grid and 12 vertical levels (1000, 925, 850, 700, 600, 500, 400, 300, 250, 200, 150, and 100 mb). We also used NCEP reanalysis spectral-space data for surface pressure and model topography to compute the large-scale mountain torque. The mountain torque was evaluated as in Madden and Speth (1995).

b. EOF analysis

To analyze the variability of the zonal-mean zonal wind, we performed EOF analysis on the monthly wind anomalies from 10° to 80°N. For the EOF analysis, the data fields were properly weighted to account for the decrease of area toward the Pole (e.g., North et al. 1982a) and the uneven spacing of pressure levels. The first and second EOFs are unique according to the North et al. (1982b) test. We present the EOFs in meters per second and not in normalized form so that the magnitude of the structures can easily be seen. This is done by a regression of the monthly anomaly data on the normalized principal component (PC) time series. Since the PC time series of the vertical-average zonal wind anomalies is practically identical to the PC time series of the variability in the latitude–pressure plane, we will only use the EOFs of the vertical-average zonal wind.

The EOF analysis of this paper is different than the Southern Hemisphere study of LH01 in two ways. First, monthly anomalies rather than daily anomalies are used. While the choice of monthly or daily data does not effect the leading EOF of the Southern Hemisphere, it does have an effect on the leading EOF of the Northern Hemisphere north of 65°N—the center of action at 72.5°N is significantly stronger for daily data than for monthly data. Since the focus of this study is on low-frequency variability, the monthly EOF pattern will be used. Second, since we are focusing on internal atmospheric variability in the extratropics, we remove the zonal wind and eddy forcing variability that is linearly related to ENSO. This method works well because the zonal-mean response to ENSO is basically linear (Hoerling et al 1995). The zonal-mean response to ENSO is strongest in the subtropics (Fig. 1) and is evaluated using the multivariate ENSO index (MEI; Wolter and Timlin 1993, 1998). By removing the ENSO signal, the centers of action of the leading zonal wind EOF move poleward by about 2.5° and the correlation with the northern annular mode index (Thompson and Wallace 2000) increases from 0.78 to 0.88. (Once again, removing ENSO variability has little effect on EOF1 of the zonal-mean zonal wind in the Southern Hemisphere.)

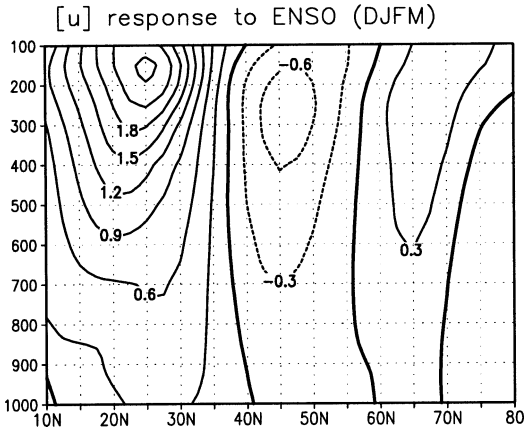

FIG. 1. Zonal-mean zonal wind regressed on monthly ENSO time series (DJFM).

c. Time series analysis

To analyze the daily momentum budget for the time series analysis, we found daily anomaly data for the zonal-mean wind, the eddy momentum flux convergence, and the large-scale mountain torque by removing the mean seasonal cycle. The mean seasonal cycle is defined as the annual average and the first four Fourier harmonics of the 25-yr (1976–2001) daily climatology. In addition, to be consistent with the EOF analysis, we removed the portion of the daily anomalies linearly related to ENSO [the monthly MEI index (section 2b) was linearly interpolated to daily resolution for this removal]. We project the vertical average (monthly) EOFs onto the daily anomaly data in order to diagnose the forcing of the zonal wind anomalies. This gives a daily time series for zonal wind, eddy momentum flux forcing, and mountain torque forcing for each EOF mode.

For the spectral analyses, we found the spectra for each 121-day winter season (DJFM) and windowed by a Hanning window. For 25 winters, this gave at least 50 degrees of freedom for the composite spectrum. We also used cross-spectrum analysis to find the phase relationship between two time series as a function of frequency. For this analysis, the coherence squared func-

tion is a measure of the consistency of the phase and amplitude relationship between the two time series over the sample.

d. Definition of synoptic and quasi-stationary eddies

To better understand the dynamics of the zonal wind variability, we divide the eddies into three parts: the ''synoptic,'' ''quasi-stationary,'' and ''residual'' eddies. First we divide the eddy components of u, v and T into high-frequency, low-frequency, and quasi-stationary parts: $u' = u'_h + u'_l + u'_s$, $v' = v'_h + v'_l + v'_s$, and $T' = T'_h + T'_l + T'_s$. The high-frequency eddies are found using a 15-day cutoff high-pass Lanczos filter with 41 weights (Hamming 1989) and the quasi-stationary eddies are found using a 40-day cutoff low-pass Gaussian-shaped filter with 45 weights. We use a Gaussian filter for the quasi-stationary eddies because the negative weights of the Lanczos filter give a noticeable artifact in the cross-covariance function (although the same general conclusions are independent of the filter choice). The low-frequency eddies are defined to be the remainder after the high-frequency and quasi-stationary eddies are removed. We define $[u'_h v'_h]$ to be the synoptic eddy momentum flux and $[u'_s v'_s]$ to be the quasi-stationary eddy momentum flux. The remainder ($=[u'_h v'_l] + [u'_l v'_h] + [u'_l v'_l] + [u'_l v'_s] + [u'_s v'_l]$) is defined to be the residual eddy momentum flux. The same definitions are used for eddy temperature flux by replacing u with T. The additional term in the momentum budget, the mountain torque, is included with the quasi-stationary wave forcing because it is a result of a stationary surface pressure field.

3. Time mean and EOFs

The average zonal-mean zonal wind for the NH during winter (DJFM) is shown in Fig. 2a. The zonal-mean wind is strongest at 30°N and 200 mb. The latitude of maximum zonal-mean wind shifts poleward to about 42.5°N near the surface. In NH winter, the distinction between the subtropical jet and the eddy-driven midlatitude jet is less clear compared to the SH (see LH01). Looking at the vertical-average eddy momentum flux convergence (Fig. 2b), we see that the eddies maintain the surface westerlies at 42.5°N but have no direct forcing of the jet at 30°N. Thus Figure 2 suggests that the strong jet at upper levels at 30°N is the subtropical jet and that the zonal-mean midlatitude jet is at a latitude of about 42.5°N where the strongest westerlies reach the surface. The leading EOF of the monthly vertical-average zonal-mean wind in the NH winter is a dipole with maximum wind anomalies near 32.5° and 55°N (Fig. 3a). If one looks at the upper-level or vertical-average winds there seems to be little relation between the latitudinal position of EOF1 of the NH winter and EOF1 of the SH (see LH01). Looking at the time-average low-level winds, however, one sees that the zero line of EOF1 lies at the latitude of maximum low-level winds for both hemispheres. Since low-level westerlies are a signature of the midlatitude jet, EOF1 represents variability associated with north–south displacements of the midlatitude jet both in the NH winter and in the SH. Moreover, both EOFs are well separated from EOF2 and explain a similar amount of the month-to-month variance (SH—52%, NH—48%).

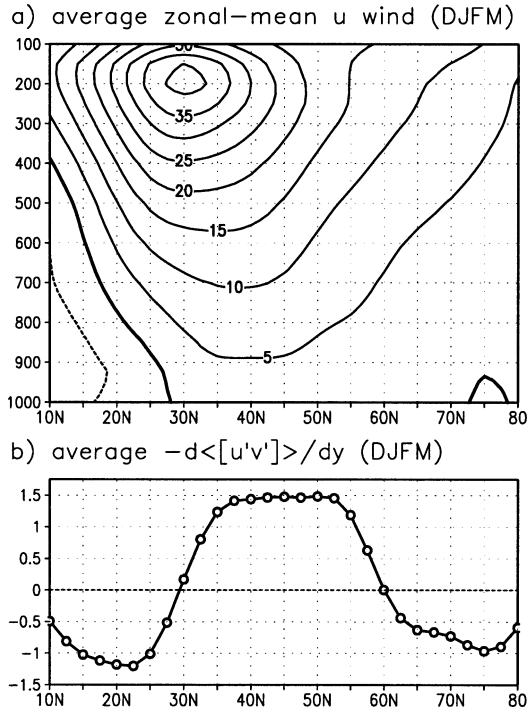

FIG. 2. (a) Time- and zonal-mean zonal wind (DJFM). (b) Time-, vertical-, and zonal-mean eddy momentum flux convergence in m s^{-1} day^{-1}. Spherical effects are taken into account.

EOF2 (Fig. 3b) of the zonal-mean wind is in quadrature with EOF1 and explains 29% of the monthly variance. The positive (negative) phase of EOF2 represents the strengthening (weakening) and sharpening (broadening) of the midlatitude jet.

4. Time series analysis of momentum budget

a. Definition of time series

To diagnose the forcing of the leading EOFs, we look at the momentum budget using the dominant terms in the vertical-average momentum equation[1]:

[1] The true momentum equation should have the mass in both the tendency and eddy flux term and not in the denominator of the mountain torque term, i.e., $\langle [u] \rangle$ should be $\langle [p_s u] \rangle$, etc. The changes in momentum, however, are dominated by the wind so that (1) is a good approximation (see Madden and Speth 1995).

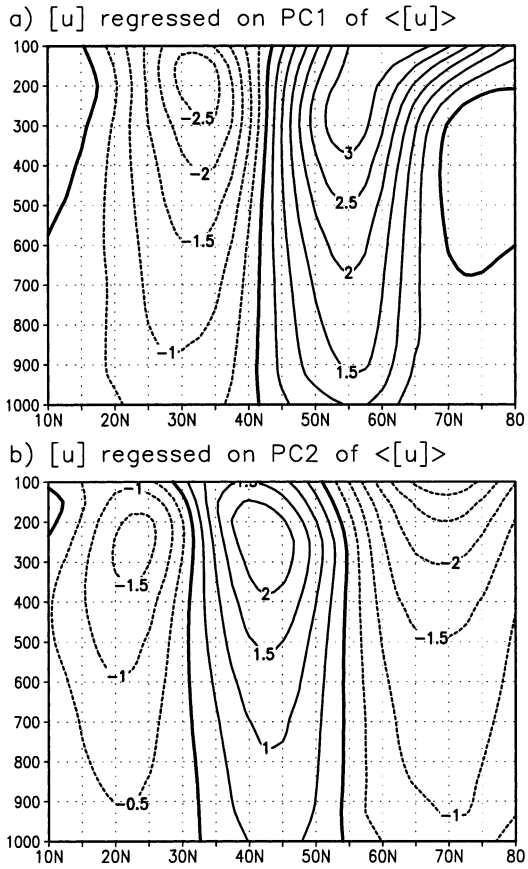

FIG. 3. Leading EOFs of monthly mean zonal wind after linearly removing ENSO variability. (a) Zonal-mean zonal wind regressed on PC1 of the vertical- and zonal-mean zonal wind using monthly data. ENSO has been linearly removed from the data. The units are m s^{-1}. (b) Same as (a) except for PC2.

$$\frac{\partial\langle[u]\rangle}{\partial t} = -\frac{1}{\cos^2\phi}\frac{\partial(\langle[u'v']\rangle\cos^2\phi)}{a\partial\phi} - \frac{g}{p_0}\left[p_s\frac{\partial h_s}{\partial x}\right] - F, \quad (1)$$

where u is the zonal wind, g is the acceleration of gravity, p_o is a constant reference surface pressure, p_s is the surface pressure, h_s is the height of the large-scale topography, $\langle u\rangle$ is the vertical average of u, $[u]$ is the zonal mean of u, u' is $u - [u]$, ϕ is the latitude, a is the radius of the earth, and F is the residual momentum forcing. The first term on the right is the eddy momentum flux convergence and the second term on the right is the large-scale mountain torque. To diagnose the effect of the eddies on the EOFs of $\langle[u]\rangle$, we project the (monthly) EOF pattern of $\langle[u]\rangle$ onto the *daily* zonal-mean wind, eddy momentum flux convergence, and mountain torque anomalies. For the remainder of this section, $z_j(t)$ is the time series for the jth EOF of the zonal wind and $m_j(t)$ is the corresponding time series for the sum of the eddy momentum flux convergence and the (eddy) mountain torque. The time series $m_j(t)$ will be called the eddy forcing since it represents the direct effect of the eddies on the jth EOF of the vertical-average zonal wind.

b. Time series analysis

Following LH01, we find the relationship between z and m using cross-spectrum analysis. The ratio of the cross spectrum ($=MZ^*$) to the z power spectrum ($=ZZ^*$) is plotted for both EOF1 and EOF2 (Figs. 4a,d). The imaginary part is somewhat close to the angular frequency, ω, and the real part is nearly constant at low frequencies.[2] This implies that $M = (\tau^{-1} + i\omega)Z$ or, equivalently,

$$\frac{dz_j}{dt} = m_j - \frac{z_j}{\tau}, \quad (2)$$

where τ is a constant. This is the equation that would be obtained if F in (1) was parameterized by Rayleigh damping with a decay timescale of τ. This Rayleigh damping represents surface drag. The large coherence squared (Figs. 4b,e) demonstrates that (2) is a good approximation. The value for τ is calculated as in LH01 and is 6.8 days for EOF1 and 7.6 days for EOF2. Since the difference between τ for EOF1 and EOF2 seems within the range of error (estimated by partitioning the data record), we will use the average value of 7.2 days for the calculations below. Note that the observed phase difference (Figs. 4c,f) is close to the expected value of atan ($\omega\tau$) for both EOF1 and EOF2 when $\tau = 7.2$ days. Also note that the decay timescale for the NH momentum budget is smaller than that for the SH ($\tau = 8.9$ days, see LH01) which is consistent with greater land surface in the NH compared to SH and therefore higher drag.[3]

The daily time series of EOF1 has about 1.7 times the power of EOF2 at the lowest frequencies but basically the same amount of power as EOF2 at frequencies above 1/40 days (Fig. 5a). Thus, EOF1 anomalies are significantly more persistent than those of EOF2 (Fig. 5b). The cross correlation between the wind anomalies and their corresponding forcing is shown in Fig. 5c. As expected from (1) and demonstrated in Figs. 4c,f, the largest correlations occur when the eddies (m) lead the zonal wind (z). Thus, the eddies cause the zonal wind anomalies. To find evidence for a feedback of the

[2] Figure 4 implies that the imaginary part of the cross spectrum is too large [i.e., the equation should be $dz/dt = (1 - \delta)m - z/\tau$, where δ is a small constant]. Perhaps the interpolation of data to pressure surfaces below topography is giving a spurious eddy momentum flux, since this effect is not observed in the SH (see LH01). This effect does not affect the simple model used in the next section because we are only interested in the changes in variability relative to observed (i.e., we can divide all the equations in the simple model by a constant and not change the results).

[3] The large-scale mountain torque has been included in the eddy forcing and is therefore not included in τ.

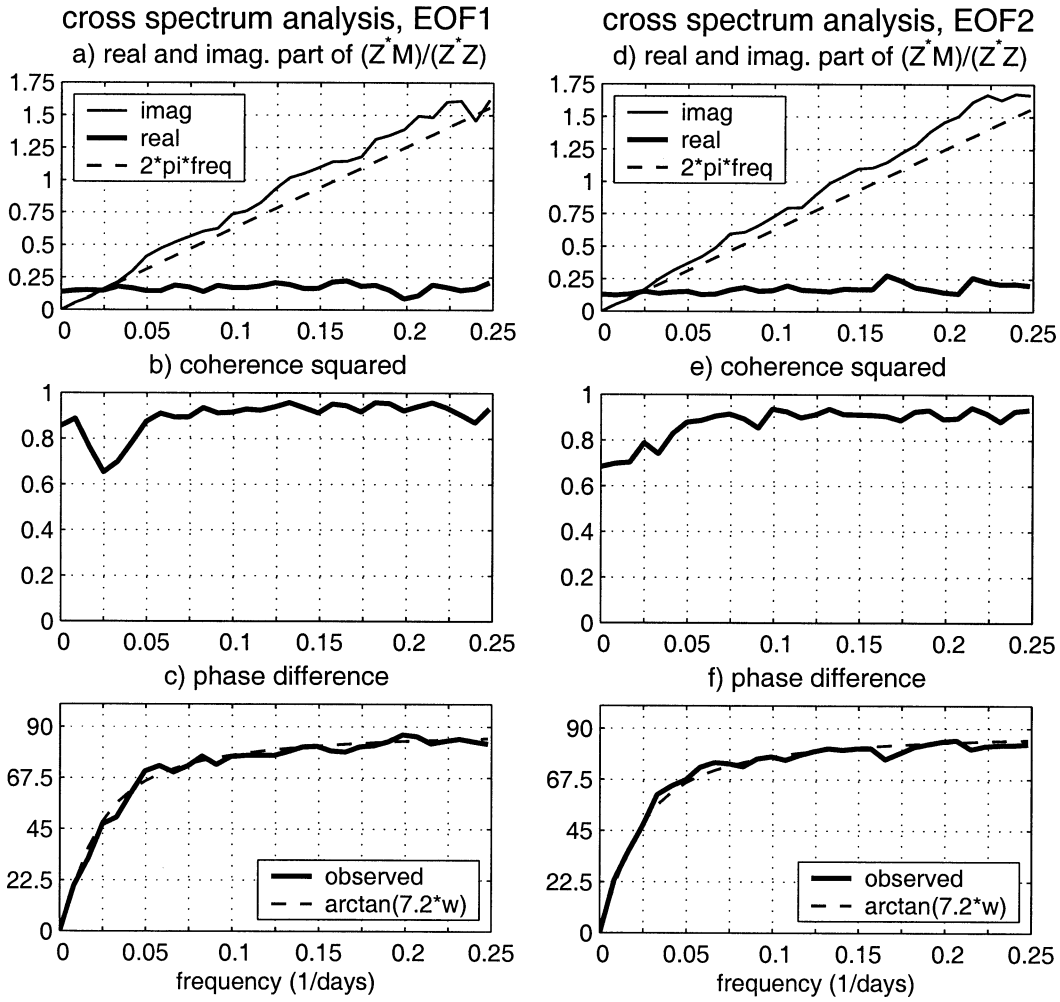

FIG. 4. Cross-spectrum analysis between the PC of the zonal wind and its eddy forcing. (a) The cross spectrum of PC1 and its eddy forcing divided by the PC1 power spectrum. Both the real and imaginary parts are shown as well as 2π times the frequency (dotted line). (b) Coherence squared function for PC1 and its eddy forcing. (c) Phase difference (°) between PC1 of the zonal wind and its eddy forcing (solid line) and an estimate of the phase difference using (2) with $\tau = 7.2$ days (dotted line). Positive phase difference means the eddy forcing leads the zonal wind. (d), (e), (f) Same as (a), (b), and (c) except for PC2 instead of PC1.

zonal wind anomalies on the eddies, LH01 argued that one must look for significant correlations at large positive lags (i.e., beyond an eddy lifetime). The assumption implicit in this argument is that without the low-frequency variability of the zonal-mean flow, the eddies have no long-term memory. In this case, the correlations are small but consistently positive at large lags for both EOF1 and EOF2 with EOF1 having a significantly stronger feedback. For EOF1, the correlations implying a positive feedback are significant at the 95% significance level at lags up to 22 days (see appendix B of LH01), while for EOF2 the correlations are significant from lags 8 to 14 days. In addition, the positive correlations for both EOF1 and EOF2 are reproducible in subsamples of the data record suggesting that the correlations are real. Before we apply the quantitative model of LH01, we review the argument in LH01 that positive correlations imply a positive feedback.

Positive correlations imply a positive feedback if one assumes that without the low-frequency variability of the zonal-mean wind the eddies have no long-term memory. While this assumption seems reasonable in the SH where the momentum budget is dominated by transients, it is less clear whether this assumption holds true in the NH, where large-scale quasi-stationary waves play an important role in the momentum budget (see DeWeaver and Nigam 2000a). We find, however, that the same argument in the SH applies in the NH. First we divide the eddies into the synoptic eddies and everything else (see section 2d) as in LH01. We then compare the contribution of the synoptic eddies to the lag covariance between the zonal wind and the *total* eddy forcing.

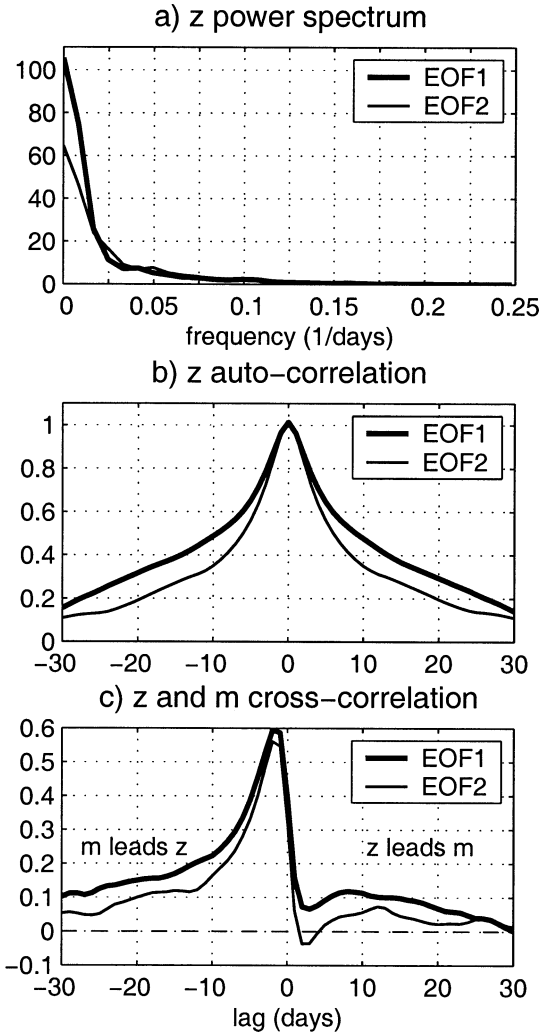

FIG. 5. (a) Power spectrum for PC1 and PC2 of the vertical- and zonal-mean zonal wind. (b) Autocorrelation for PC1 and PC2 of the vertical- and zonal-mean zonal wind. The *x* axis is time lag in days. (c) Cross correlation between PC1 and its eddy forcing (thick line) and PC2 and its eddy forcing (thin line). Positive time lag means PC1 (zonal wind) leads the eddies (*m*).

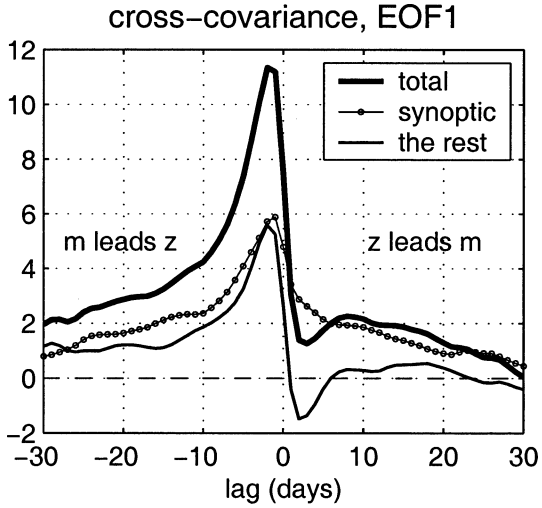

FIG. 6. Cross covariance between PC1 of the zonal wind and various components of the eddy forcing. The thick line is for the total eddy forcing, the line with dots is for the synoptic eddy forcing, and the thin line is for the total eddy forcing minus the synoptic eddy forcing. Positive time lag means the zonal wind leads the eddies.

Looking at Fig. 6 we see that the synoptic eddies clearly dominate the cross covariance at large positive lags. Since the synoptic eddies consist of fluctuations in u' and v' of periods less than 15 days, yet they provide the memory in the cross-covariance function, the synoptic eddy forcing must be organized by the changes in the zonal-mean wind. Consequently, the correlations at large positive lags in Fig. 5c are due to a positive feedback with the zonal-mean wind.

c. Simple model of feedback

We now use the simple model described in LH01 to determine whether the strength of the positive feedback accounts for the increased persistence of EOF1 compared to EOF2. Using cross-spectrum analysis, we empirically found that the *time series* z_j and m_j are related by (2), where the index j refers to either EOF1 or EOF2. We take τ to be 7.2 days. To model the eddy feedback, assume that the changes in zonal wind cause an eddy forcing *anomaly* proportional to the wind *anomaly*, that is, assume

$$m_j = \tilde{m}_j + b_j z_j, \tag{3}$$

where $\tilde{m}_j$ will be called the ''random'' eddy forcing because this forcing is not caused by the zonal wind *anomaly* and b_j is a constant that measures the strength of the feedback. Let $\tilde{z}_j$ be the zonal wind time series in the absence of the feedback. Thus, if we assume that τ does not depend on the feedback, then $\tilde{z}_j$ must be defined by

$$\frac{d\tilde{z}_j}{dt} = \tilde{m}_j - \frac{\tilde{z}_j}{\tau}. \tag{4}$$

LH01 derive the cross covariance between $\tilde{z}_j$ and $\tilde{m}_j$ from the observed cross covariance (i.e., between z_j and m_j) using (2), (3), and (4). The constant b_j is determined such that the cross covariance ''without the feedback'' is zero when $\tilde{z}_j$ leads $\tilde{m}_j$ by over a week.

We now use this simple model to determine if the strength of the positive feedback accounts for the difference between EOF1 and EOF2 (see the appendix). Figure 7 shows the effect of decreasing the feedback for EOF1 ($=b_1$) to the value for EOF2 ($=b_2$). We see that the strength of the positive zonal wind–eddy feedback basically accounts for the difference in the persistence (Fig. 7b) and variance (Fig. 7c) between EOF1 and EOF2. The main result of this section is that the leading EOF of extratropical variability is selected by the eddy–zonal flow feedback. Without the feedback, the variability would be uniform in latitude because the

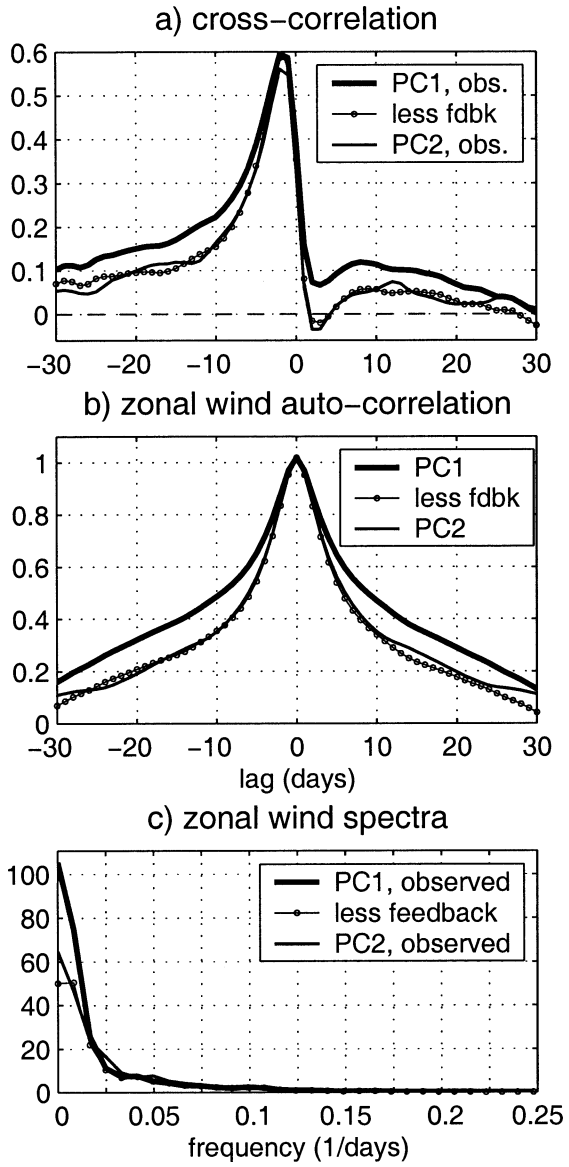

FIG. 7. The effect of the stronger eddy–zonal wind feedback on the PC1 variability calculated from the simple model. (a) Same as Fig. 5c except that the calculated curve with the PC1 feedback reduced is also included (line with dots). (b) Same as Fig. 5b except that the calculated curve with the PC1 feedback reduced is also included (line with dots). (c) Same as Fig. 5a except that the calculated curve with the PC1 feedback reduced is also included (line with dots).

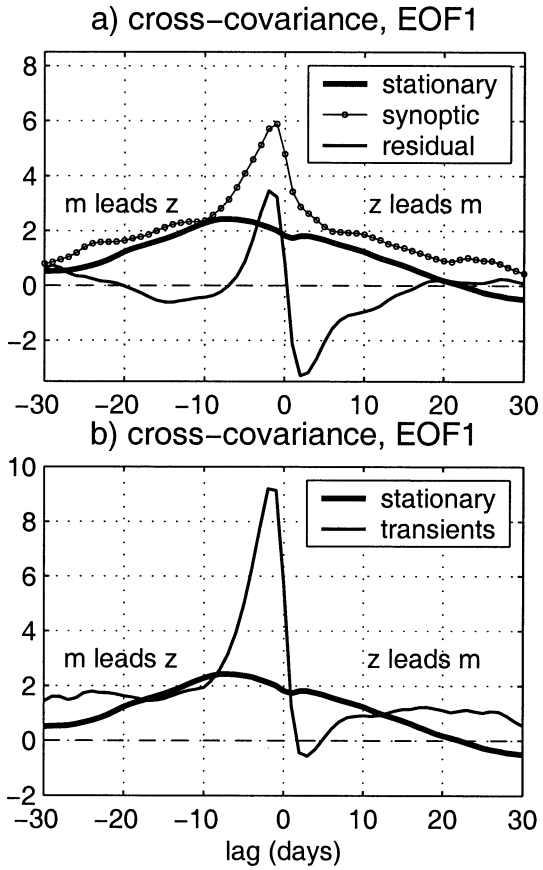

FIG. 8. Cross covariance between PC1 of the zonal wind and various components of the eddy forcing of PC1. Positive time lag means the zonal wind leads the eddies. (a) The thick line is for the quasi-stationary eddy forcing (including mountain torque), the line with dots is for the synoptic eddy forcing, and the thin line is for the residual eddy forcing (i.e., everything else). (b) The thick line is for the quasi-stationary eddy forcing (including mountain torque), the thin line is for the transient eddies (i.e., total minus quasi-stationary).

random part of the eddy forcing drives both EOF1 and EOF2 equally. Since the positive feedback distinguishes the leading EOF above other patterns, we focus on the eddy anomalies after the peak in the zonal winds despite the fact that the strongest correlations occur when the eddies lead the zonal wind anomalies.

5. Stationary waves and synoptic waves

In the previous section, we saw that the synoptic eddies seem to dominate the eddy response to the zonal wind anomalies. To get a more complete description of the response it is useful to further divide the remaining eddies using time filtering (see section 2d) into quasi-stationary and residual eddies. Thus, the eddy forcing consists of three parts: the synoptic eddies, the quasi-stationary eddies, and the residual eddies (i.e., everything else). The cross covariance between PC1 of the zonal wind and these three forcings (Fig. 8a) allows us to compare the contribution to the positive feedback. Looking at the response to the zonal wind anomalies (i.e., positive lags beyond an eddy lifetime) we see that the synoptic and quasi-stationary eddies reinforce the wind anomalies whereas the residual eddies damp the wind anomalies. The synoptic and residual eddies play the same role in the SH zonal wind variability (the residual eddies include *all* low- and cross-frequency eddies in the SH instead of just the medium range as in the NH). In the NH, unlike the SH, the eddies with the lowest frequencies reinforce the zonal wind anomalies.

Still, the synoptic eddies contribute the most to the eddy response to the zonal wind anomalies.

To help compare our results with previous studies we also include Fig. 8b, which shows the transient eddy forcing (= sum of synoptic and residual eddies). The transient and quasi-stationary eddies contribute a similar amount to the positive feedback although the transient eddy forcing is more persistent than the quasi-stationary eddy forcing. The reason the quasi-stationary waves play a smaller role than that suggested by DeWeaver and Nigam (2000a) is that we project the EOF1 weighting function onto the eddy-forcing anomalies in order to calculate the positive feedback. We will see in the next section that although the quasi-stationary eddies have a large response to the zonal wind anomalies, their forcing does not project well onto the wind anomalies. Instead the quasi-stationary eddy response tends to move the zonal wind anomalies poleward. In addition, the quasi-stationary eddy forcing also includes the mountain torque, which tends to damp the wind anomalies (Fig. 12b).

6. Dynamics of the feedback

a. Preliminaries

In order to diagnose the effect of the zonal-mean wind anomalies on the eddies, we must look at time-lagged regressions rather than simultaneous or monthly mean regressions. The reason for the time lag is to isolate the part of the eddy forcing that is responding to the zonal wind anomalies from the burst of eddy forcing that initially created the zonal wind anomalies (Feldstein and Lee 1996, 1998; Lee and Feldstein 1996; Robinson 1996; LH01). The time lag is very important because the shapes of the patterns and the relative size of the vertical and horizontal Eliassen–Palm (EP) flux (Edmon et al. 1980) depend on the sign of the time lag. For the following figures, we average the eddy anomalies over time lags from 8 to 30 days (zonal wind leads eddies). The precise time lag is not important as long as it is greater than an eddy lifetime (here taken to be 1 week).

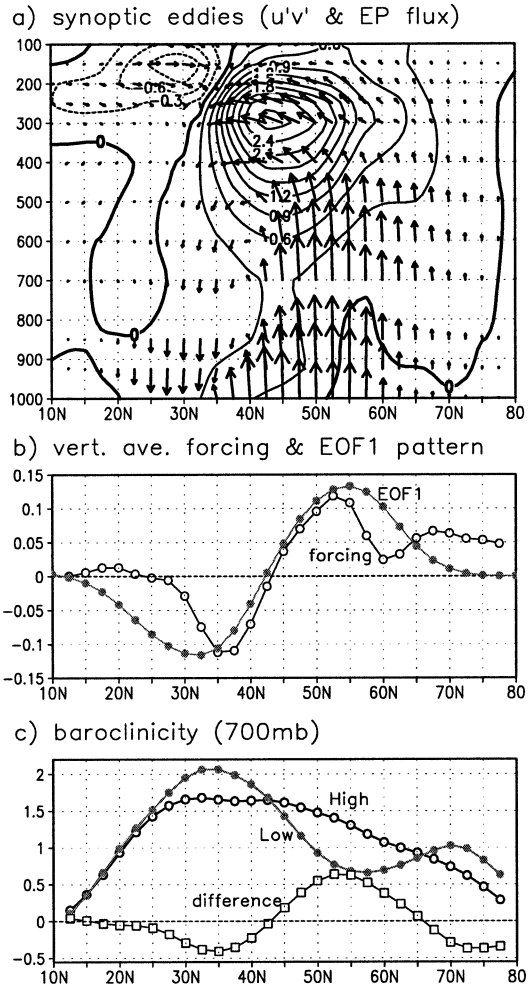

FIG. 9. Synoptic eddy response to the PC1 wind anomalies. (a) Lag regression of the $[u'v']\cos\phi$ (contours) and EP flux (vectors) anomalies by the synoptic eddies. The plot is averaged over time lags from 8 to 30 days (PC1 of the wind leads eddies). (b) Lag regression of the vertical-average synoptic eddy forcing (open circles; units are m s^{-1} day^{-1}). The curve is averaged over time lags from 8 to 30 days. The EOF1 weighting pattern (solid circles) is included for reference (arbitrary units). (c) The composite baroclinicity during the high (open circles) and low (closed circles) index as well as the difference (open squares; high minus low index).

b. Synoptic eddies

The synoptic eddy response to the EOF1 zonal wind anomalies consists of strong $[u'v']$ anomalies across the node of EOF1 (42.5°N) and weaker $[u'v']$ anomalies in the subtropics (Fig. 9). These $[u'v']$ anomalies tend to reinforce the zonal-mean wind anomalies associated with EOF1. The $[u'v']$ across 42.5°N are associated with corresponding changes in the vertical EP flux both north and south of 42.5°N. The vertical EP flux anomalies north of 42.5°N are considerably stronger than those south of 42.5°N and are of the opposite sign. These EP flux anomalies imply stronger baroclinic wave generation in the region of stronger westerlies especially in the high index. Looking at the composite ''baroclinicity'' $[=(g\theta_y)/(\theta_0 N)$, this is proportional to the Eady (1949) wave growth rate] during the high and low index (Fig. 9c), we see that the changes in baroclinicity are roughly consistent with the changes in the vertical EP flux. Moreover, the changes in baroclinicity are stronger north of 42.5°N than south of 42.5°N, which is the same sense as the asymmetry in the vertical EP flux, although not as strong.

In the SH, lag regressions show that the vertical EP flux anomalies are basically symmetric about the node of the zonal wind anomaly (see Fig. 8 in LH01), while in the NH the vertical EP flux anomalies are much stronger on the poleward side of the node. If the annular mode index [i.e., PC1 of the 1000-mb geopotential

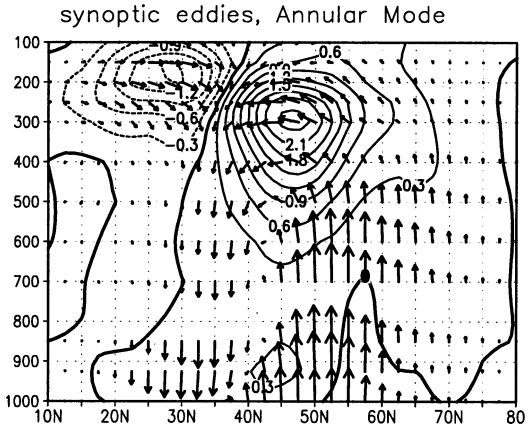

FIG. 10. Synoptic eddy response to the annular mode. Lag regression of the $[u'v']$ cosϕ (contours) and EP flux (vectors) anomalies by the synoptic eddies. The plot is the averaged over time lags from 8 to 30 days (annular mode leads eddies).

height (with no zonal averaging)] is used instead of PC1 of $\langle[u]\rangle$, however, this asymmetry is more reduced: the ratio of the vertical EP flux poleward of the node to that equatorward decreases from 3.5 for PC1 to 1.3 for the annular mode (Fig. 10). (We use the amplitude of the vertical EP flux at 500 mb as representative of the flux entering the upper troposphere.) The changes in baroclinicity are also more symmetric using the annular mode (AM). Thus, it appears that Atlantic variability (which is emphasized in the AM index) is more like the zonal-mean variability in the SH and zonally symmetric GCMs, which might partly explain the dominance of the Atlantic sector over the Pacific sector in the NH annular mode. We will return to this point in the discussion.

The main points of this section are that 1) changes in $[u'v']$ are associated with changes in the source of synoptic waves and 2) these changes in the source of synoptic waves are roughly consistent with the changes in the baroclinicity.

c. Residual eddies

The long-term response of the residual eddies to the zonal wind anomalies is dominated by waves in the 15–40-day period range rather than the ''cross-frequency'' terms of the residual eddy fluxes. The residual eddy momentum flux anomalies are strongest near the node of EOF1 and are in a direction that tends to damp the zonal wind anomalies (Fig. 11). The structure of the residual eddy $[u'v']$ pattern in the midlatitudes is significantly more barotropic than the synoptic eddies: the amplitude of the fluxes varies by a factor of 2 between the upper and lower troposphere for the residual eddies, while for the synoptic eddies the amplitude varies by a factor of 9 (see Fig. 9). The deep vertical structure of the $[u'v']$ anomalies suggests that these waves are predominantly external Rossby waves (Held et al. 1985).

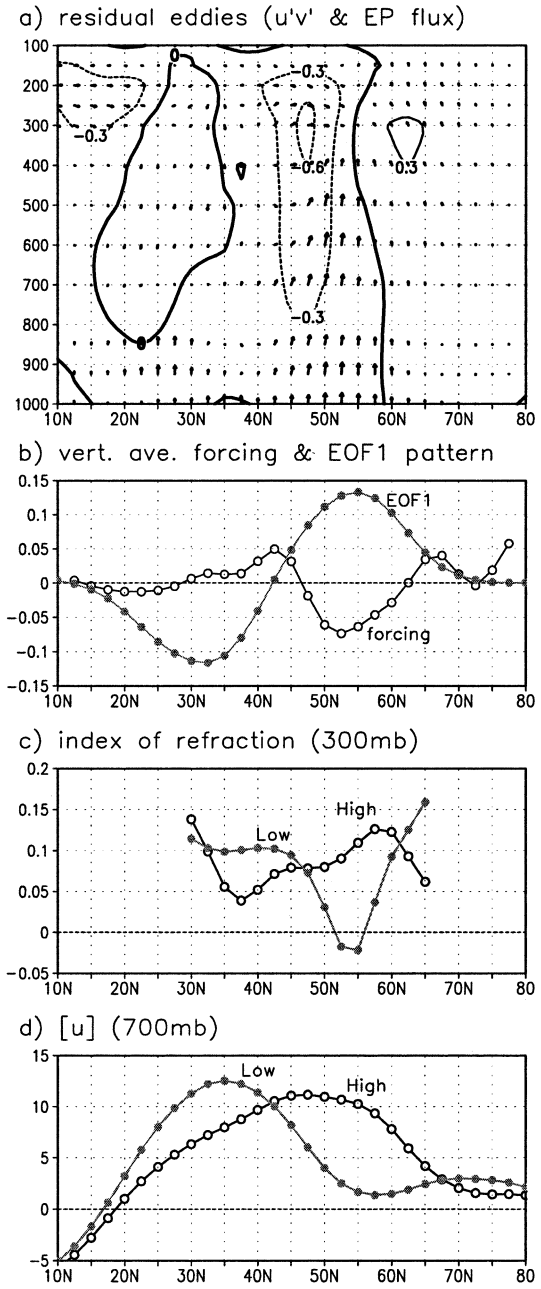

FIG. 11. Residual eddy response to the PC1 wind anomalies. (a) Lag regression of the $[u'v']$ cosϕ (contours) and EP flux (vectors) anomalies by the residual eddies. The plot is the averaged over time lags from 8 to 30 days (PC1 of the wind leads eddies). (b) Lag regression of the vertical average residual eddy forcing (open circles; units are m s^{-1} day^{-1}). The curve is averaged over time lags from 8 to 30 days. The EOF1 weighting pattern (solid circles) is included for reference (arbitrary units). (c) The composite index of refraction (see text for definition) during the high (open circles) and low (closed circles) index. The index of refraction is only plotted where the eddies are nearly barotropic. (d) The composite zonal-mean wind at 700 mb during the high (open circles) and low (closed circles) index.

External Rossby waves are trapped in the tropospheric ''waveguide'' and therefore consist of a superposition of equal amounts of upward- and downward-propagating waves. This simplifies the dynamics in that the relevant index of refraction is $(\beta - u_{yy})/(u - c)$ at a *single* ''equivalent barotropic level'' (Held et al. 1985). Composites during the high and low index days (Fig. 11c) show that the external Rossby wave index of refraction is basically largest in the jet. Thus, external Rossby waves tend to propagate poleward across 45°N during the high index and equatorward across 45°N in the low index. Outside the midlatitudes the wave anomalies are not barotropic, so the simplified index of refraction does not apply.

In summary, the jet is a waveguide for external Rossby waves (see also Hoskins and Ambrizzi 1993; Yang and Hoskins 1996). Therefore, external Rossby waves tend to propagate into the jet and, since wave momentum transport is opposite to wave propagation, remove momentum from the jet.

d. Quasi-stationary eddies

In the midlatitudes of the SH, the anomalies by the low-frequency waves look like external Rossby waves (see Fig. 9 of LH01). In the Northern Hemisphere, a portion of these anomalies also look like external Rossby waves (the residual eddies), but the fluxes by the very low frequency ($<$1/40 days^{-1}) waves have a very different structure: the $[u'v']$ is concentrated at upper levels and the vertical EP flux anomalies are much larger (Fig. 12). The reason for the difference between the NH and SH are the strong stationary wave sources in the midlatitudes of the NH compared to the SH. Near stationary wave sources, the wave field consists of a full spectrum of waves. It is only away from wave sources that the dispersion of excess wave activity and reflections within the tropospheric waveguide set up an external Rossby wave field (Held 1983; Held et al. 1985). Thus in the NH, waves at very low frequency (e.g., waves that are stationary or nearly stationary) are dominated by waves dispersing from midlatitude wave sources rather than external Rossby waves. In the NH, it is only in the medium-frequency range that external Rossby waves dominate over other waves generated locally (either by stationary sources or by baroclinic instability).

The vertical-average forcing by the quasi-stationary waves is very strong especially poleward of 55°N (Fig. 12b), which agrees with DeWeaver and Nigam (2000a). However, this strong forcing does not project well onto the EOF1 wind anomalies. The positive feedback by the quasi-stationary waves is mixed with a response that tends to move the anomalies poleward (see also Feldstein 1998). Also note that the mountain torque anomalies (due to Greenland) tend to damp the forcing by $[u'v']$ north of 60°N. [The effect of the mountain torque on the $[u'v']$ forcing (open circles) is shown by the open squares.] Because of the less-than-optimal projection of quasi-stationary wave forcing onto EOF1 and the stationary eddy mountain torque, the quasi-stationary waves do not dominate the positive feedback associated with EOF1.

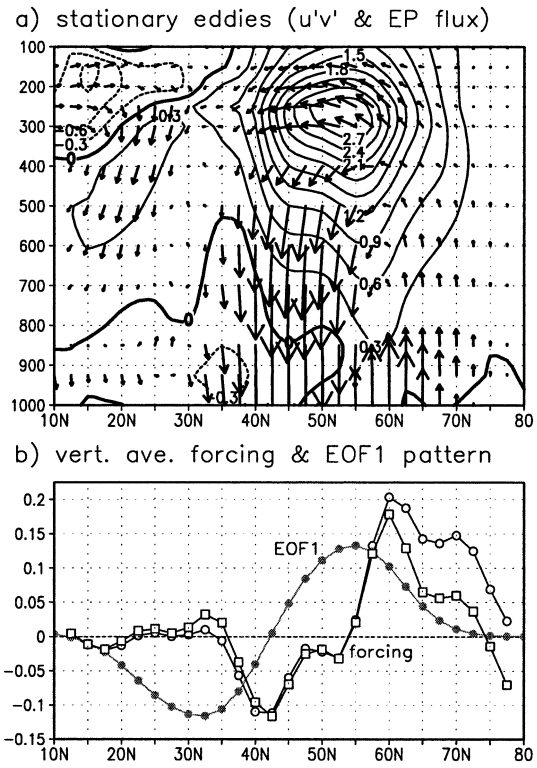

FIG. 12. Quasi-stationary eddy response to the PC1 wind anomalies. (a) Lag regression of the $[u'v']\cos\phi$ (contours) and EP flux (vectors) anomalies by the quasi-stationary eddies. The plot is the averaged over time lags from 8 to 30 days (PC1 of the wind leads eddies). (b) Lag regression of the vertical average quasi-stationary eddy forcing by $[u'v']$ (open circles) and by both $[u'v']$ and the mountain torque (open squares; units are m s^{-1} day^{-1}). The curves are averaged over time lags from 8 to 30 days. The EOF1 weighting pattern (solid circles) is included for reference (arbitrary units).

At first, Fig. 12a suggests the following explanation for the quasi-stationary eddy forcing: the anomalous source of wave activity around 45° during the low index leads to the anomalous propagation of wave activity away from the source latitude (and the observed $[u'v']$ anomalies). Looking more carefully, however, we see evidence that suggests other mechanisms may be more important. First, when we divide the total quasi-stationary wave into contributions from the Atlantic and Pacific sectors (Fig. 13; 90°E and 90°W are the dividing longitudes) we see that the vertical EP flux is concentrated in the Pacific sector while the horizontal EP flux is concentrated in the Atlantic sector. Moreover, the horizontal EP flux anomalies in the upper troposphere in the Atlantic are stronger than the EP flux anomalies below (e.g., 500 mb) so that the horizontal EP flux anomalies appear discontinuous from the wave sources

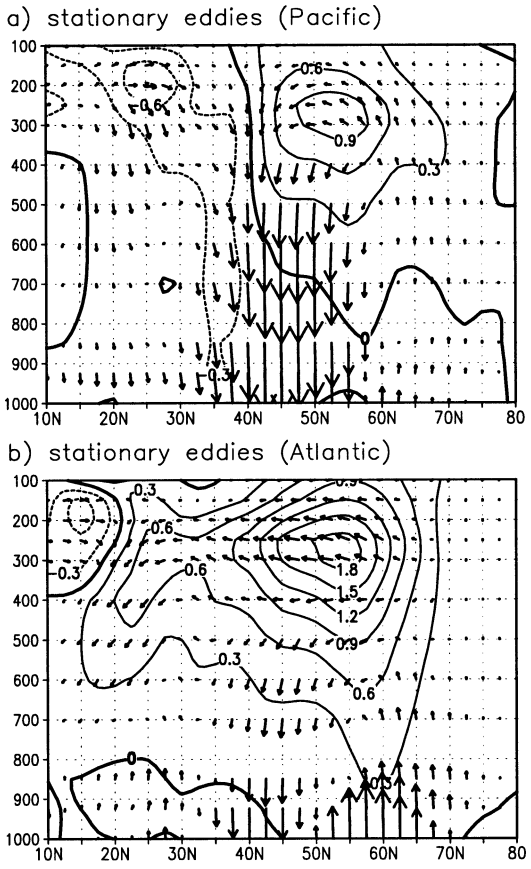

FIG. 13. The two components of the quasi-stationary eddy response to the PC1 wind anomalies. (a) Lag regression of the $[u'v']\cos\phi$ (contours) and EP flux (vectors) anomalies by the quasi-stationary eddies in the Pacific sector. (b) Lag regression of the $[u'v']\cos\phi$ (contours) and EP flux (vectors) anomalies by the quasi-stationary eddies in the Atlantic sector. Both plots are the averaged over time lags from 8 to 30 days (PC1 of the wind leads eddies).

at low levels.[4] Because the majority of the anomalies in the horizontal EP flux seem to be independent of changes in the wave source, it appears that changes in the zonal-mean flow in the mid- to upper troposphere are most important (i.e., changes in the refractive index).

To help explain the quasi-stationary wave forcing we use the zonal-mean quasigeostrophic refractive index (Matsuno 1970) for waves with zero frequency:

$$n^2 = \frac{[q]_\phi}{[u]} - \left(\frac{k}{a\cos\phi}\right)^2 - \left(\frac{f}{2NH}\right)^2, \qquad (5)$$

where

$$[q]_\phi = \frac{2\Omega}{a}\cos\phi - \frac{1}{a^2}\left\{\frac{([u]\cos\phi)_\phi}{\cos\phi}\right\}_\phi - \frac{f^2}{\rho_0}\left(\rho_0\frac{[u]_z}{N^2}\right)_z. \qquad (6)$$

Here, k is the zonal wavenumber, ω is the wave frequency, N is the buoyancy frequency, H is the scale height (8 km), f is the Coriolis parameter, a and Ω are the earth's radius and angular frequency, ρ_0 is the background density, and ϕ is latitude. Waves can propagate in regions of positive refractive index and waves are evanescent in regions of negative refractive index (lightly shaded in Fig. 14). Also, waves tend to be refracted toward large positive refractive index. Since the refractive index for stationary wavenumbers 1 and 2 are very similar, we only show the results for wavenumber 1 below.

In the upper troposphere, the most prominent difference between the high and low phase of PC1 is the large refractive index north of 57.5°N at 500–400 mb during the low phase (Fig. 14; see also Limpasuvan and Hartmann 2000). As noted by Limpasuvan and Hartmann (2000), the large quasi-stationary wave forcing poleward of 57.5°N bears a striking resemblance to the large difference in refractive index between the high and low phases of PC1. The difference between the low and high phase (Fig. 14c) shows a large increase as one moves poleward across 57.5°N much like the vertical-average quasi-stationary wave forcing (Fig. 12b). During the low phase of PC1, this region of increased refractive index tends to attract wave activity leading to an easterly momentum forcing in this region (Limpasuvan and Hartmann 2000). Chen and Robinson (1992) studied the effect of a very similar refractive index profile on quasi-stationary waves in a linear primitive equation model and found similar results. Essentially, a region of high refractive index is a wave sink. In the low phase of PC1, the high latitudes are a more effective sink of wave activity.

To find the zonal-mean flow characteristics most important for giving the observed refractive index we rewrite (6) in the following form:

$$[q]_\phi = \underbrace{\frac{2\Omega}{a}\cos\phi - \frac{1}{a^2}\left\{\frac{([u]\cos\phi)_\phi}{\cos\phi}\right\}_\phi} + \underbrace{\frac{f^2}{N^2}\left((\ln N^2)_z[u]_z + \frac{[u]_z}{H}\right)} - \underbrace{\frac{f^2}{N^2}u_{zz}}. \qquad (7)$$

The first set of terms on the right will be called the meridional curvature term, the second set will be called the vertical shear term, and the third set will be called the vertical curvature term. In addition, the $[u]$ dividing $[q]_\phi$ in (5) will be called the zonal wind in the denominator term. To find the effect of a particular term for

[4] Remember that these EP fluxes are anomalies. The sum of the time-mean and the anomalies still implies a lower-tropospheric source.

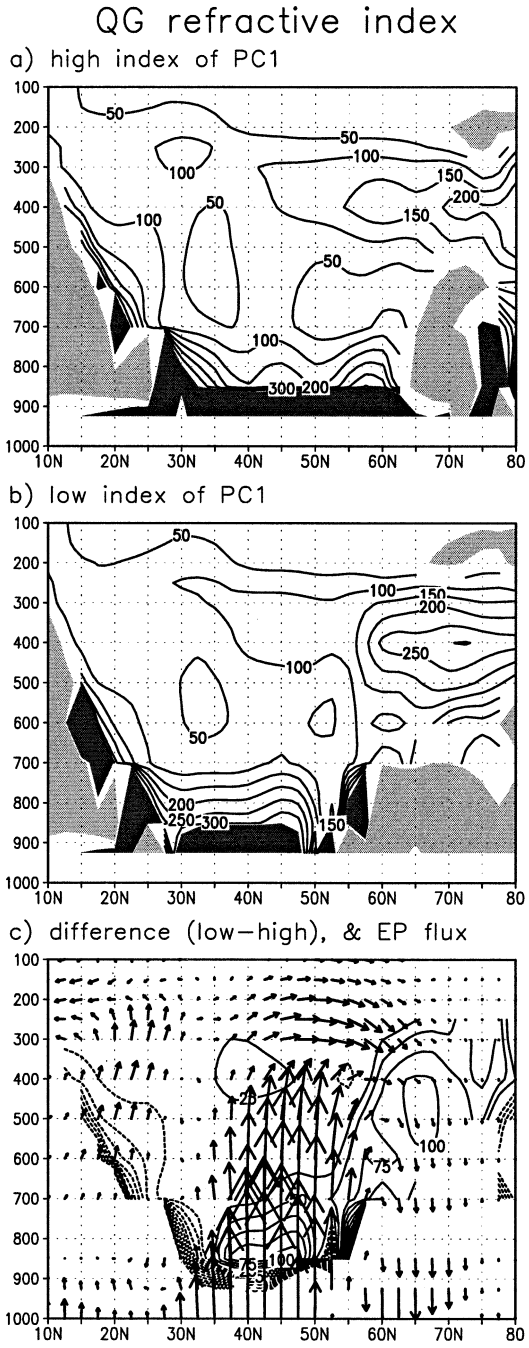

FIG. 14. Quasi-geostrophic refractive index by stationary wave 1: (a) high index, (b) low index, (c) low minus high index. The values are nondimensionalized by the radius of the earth squared. Negative values are lightly shaded and values larger than 300 are black in (a) and (b). The quasi-stationary EP flux anomalies from Fig. 11a are also shown (with the reverse sign).

giving the observed changes in the refractive index, we set all other terms in (5) and (7) to their climatological values and only allow the particular term to vary between the high and low phase. To help compare with previous studies, we use the annular mode index for our composites. Figure 15a shows the difference between the low phase and the high phase for the annular mode. Note that in the mid- to upper troposphere the pattern is similar to that using PC1 of $\langle [u] \rangle$ (Fig. 14c) although the difference is significantly stronger for the annular mode index. The effect of the changes in vertical shear is small and has the wrong sign (Fig. 15b). The effect of the changes in vertical curvature account for about half the observed difference (Fig. 15c). The position and shape of the pattern associated with $[u]_{zz}$ most closely resembles the observed difference than any other single term. When we include the effect of the changes in both the vertical curvature and the zonal wind in the denominator we see that we more than account for the amplitude of the refractive index anomaly (Fig. 15d) but the position of the anomaly is shifted slightly southward relative to the observations. When we include the effect of the meridional curvature term the feature moves to its proper place (not shown). In contrast to Limpasuvan and Hartmann (2000), we find that the changes in the vertical shear are *not* responsible for the observed difference in refractive index (see also Hu and Tung 2002). Looking at (7) we see that the effect of the vertical shear is opposite to the required difference: high vertical shear in the high index increases $[q]_\phi$ but the net effect of all the terms together is to decrease $[q]_\phi$ in the high index.

e. Poleward drift of zonal-mean wind anomalies

While our analysis of the momentum budget using the simple model assumes that EOF1 and EOF2 are independent, it has been shown that zonal wind anomalies tend to drift poleward in time (Feldstein 1998), which implies that there must be a consistent phase relationship between EOF1 and EOF2. The eddy momentum flux that forces this poleward drift of the wind anomalies is evident in both the synoptic and the quasi-stationary eddy forcing (see Figs. 9b and 12b). We tried to fit a two EOF simple model to the data using the same assumption as the model in this paper: there is no correlation between the zonal-mean wind anomalies and the eddy-forcing anomalies at large positive lags. Unfortunately, the model did not seem to fit the data in a consistent or sensible way. Perhaps the two EOF model has too many free parameters (four instead of one) and/or the dataset is not long enough. Fortunately, the poleward drift does not appear strong enough to interfere with the conclusions of the one EOF simple model.

To see this poleward drift we show the lag regression of the $[u]$ anomalies on PC1 at a time lag of 0 and 20 days (Fig. 16, PC1 leads $[u]$ in Fig. 16b). The poleward drift is most evident in the polar regions where the sign of the wind anomalies changes. Also note the persistence of the flow in the stratosphere in the polar night jet and the development of positive wind anomalies in the deep Tropics at 150 mb. In contrast, the poleward drift is hardly evident in the midlatitudes (see also Feld-

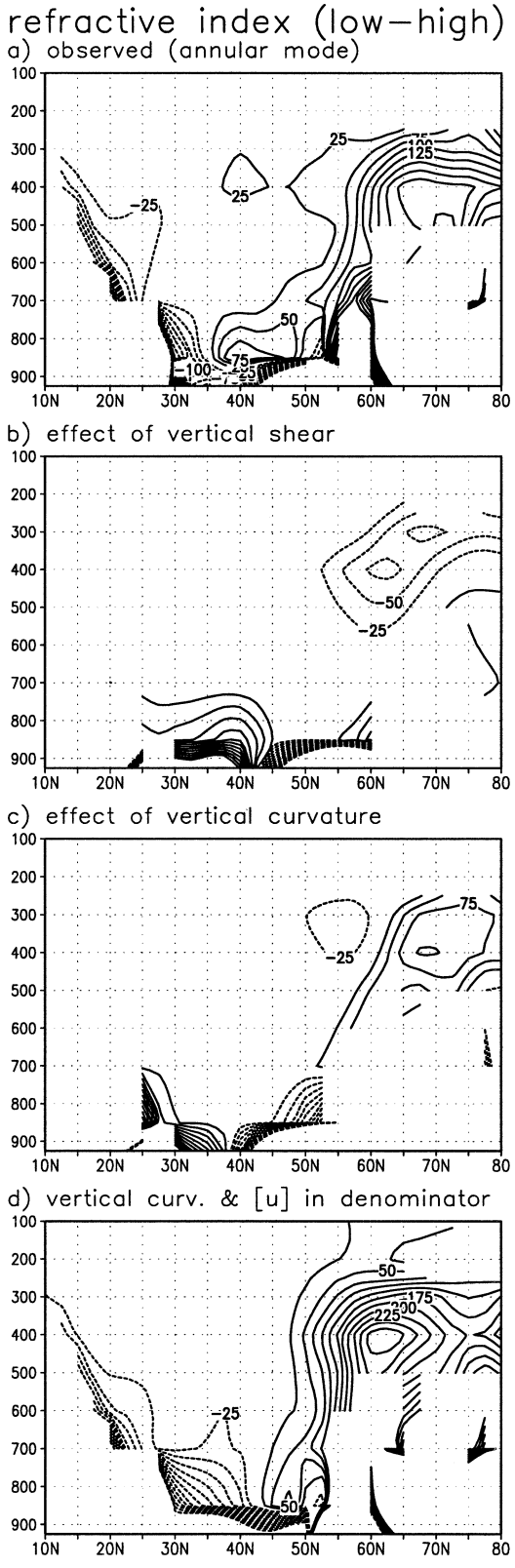

stein 1998). The poleward drift for EOF1 in the NH is considerably less than that for EOF2 in the SH (see Fig. 15 of LH01). In fact, current work using GCMs with zonally symmetric forcing suggests that EOF2 zonal wind anomalies have a strong tendency to drift poleward and become EOF1 zonal wind anomalies, while EOF1 wind anomalies are basically fixed in latitude. While this result seems to apply to the SH also, the EOF2 anomalies in the NH do *not* show a stronger tendency to propagate compared to EOF1. Since the zonal-mean response to ENSO (Fig. 1) projects heavily onto EOF2 (Fig. 3b), it seems possible that low-frequency variability in the Tropics helps fix the NH EOF2 wind anomalies in latitude.

7. Conclusions

a. Summary

The positive eddy–zonal flow feedback selects the leading pattern of extratropical variability in the NH winter. Like the SH, the synoptic (high frequency) eddies reinforce the zonal wind anomalies while external Rossby waves damp the wind anomalies. The most important difference between the hemispheres is that the quasi-stationary (frequencies $<1/40$ days^{-1}) waves reinforce the zonal wind anomalies in the NH.

The synoptic (high frequency) eddies are most important for the positive eddy–zonal flow feedback. While the quasi-stationary waves play an important role, our results imply that their role is not as important as earlier studies suggest (DeWeaver and Nigam 2000a,b; Limpasuvan and Hartmann 2000; Kimoto et al. 2001). The reason for the discrepancy is that the quasi-stationary wave response to the zonal wind does not project well onto the zonal wind anomalies. Instead the quasi-stationary wave response tends to move the wind anomalies poleward, especially at very high latitudes. Also the (stationary wave) mountain torque has a damping effect.

The mechanism of the eddy–zonal wind feedback is as follows. 1) For the synoptic eddies, changes in the source of the synoptic (baroclinic) waves appear most important. An anomalous baroclinic wave source leads to anomalous wave activity propagating from the latitude of the source. This wave propagation is accompanied by a westerly momentum flux into the source region. This is a positive feedback because (i) the source of baroclinic waves is largest in the midlatitude jet

←

FIG. 15. The difference in the quasi-geostropic refractive index by stationary wave 1 (low minus high index). The values are nondimensionalized by the radius of the earth squared. The differences are based on composites using the annular mode: (a) observed difference; (b) contribution to the observed difference by the $[u]_z$ terms, (c) contribution to the observed difference by the $[u]_{zz}$ term, (d) contribution to the observed difference by both $[u]_{zz}$ and the $[u]$ in the denominator.

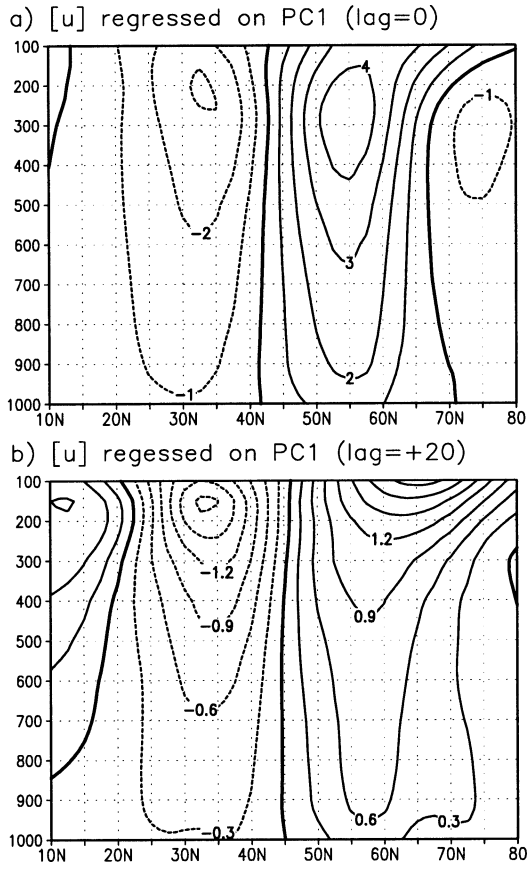

FIG. 16. Anomalous zonal-mean zonal wind regressed on PC1: (a) simultaneous, and (b) PC1 leads by 20 days.

where the baroclinicity is strongest, and (ii) the propagation of waves away from the jet at upper levels helps restore the baroclinicity of the jet via an induced mean meridional circulation (see Robinson 2000). 2) For external Rossby waves (which dominate the anomalous forcing by medium-frequency waves), the midlatitude jet is a waveguide and therefore tends to attract wave activity (Hoskins and Ambrizzi 1993; Yang and Hoskins 1996; LH01). Thus, there is a net flux of wave activity into the jet. Because westerly momentum flux is opposite to wave propagation, this is a negative feedback. 3) Presumably, external Rossby waves are also present at the lowest frequencies. In the NH, however, their effect is overwhelmed by waves generated locally (i.e., in the midlatitudes) by stationary asymmetries in topography and heating. The forcing by the quasi-stationary waves seems most effected by a strong index of refraction anomaly in the high latitudes. During the low index, the positive refractive index anomaly is a wave sink that decelerates the zonal winds there. This leads to eddy forcing in the high latitudes, which tends to both reinforce the zonal wind anomalies and also shift the zonal wind anomalies poleward.

b. Discussion

The zonal-mean variability in the NH shares a lot in common with the SH, however, certain aspects of NH variability seem clearly different from the SH and from general circulation models (GCMs) with more zonally symmetric forcing. In the NH, both EOF1 and EOF2 have a positive feedback, the distinction between EOF1 and EOF2 is in the *strength* of the positive feedback. This contrasts with the SH and GCMs with zonally symmetric forcing (e.g., those forced as in Held and Suarez 1994) where only EOF1 has a positive feedback. This feature of the NH might be explained by the fact that in the Pacific and Atlantic sectors the time-mean jet lies at different latitudes so that EOF1 variability means different things in the Atlantic and Pacific sectors (Ambaum et al. 2001). Even within the Atlantic sector alone, the axis of the time-mean flow does not lie on a latitude circle. LH01 postulate that the positive eddy–zonal flow feedback occurs for meridional shifts in the midlatitude jet (see their section 7). Therefore, in the NH, EOF1 does the best job explaining meridional shifts in the zonal-mean sense (see Figs. 2a and 3a), but because the flow is not zonally symmetric, EOF2 must pick up the rest of the feedback.

The zonal-mean variability in the NH also differs from the SH in the synoptic eddy response to the zonal wind anomalies. In the SH, lag regressions show that the vertical EP flux anomalies are basically symmetric about the node of the zonal wind anomaly. In the NH, on the other hand, the vertical EP flux anomalies are only symmetric when we use the annular mode (AM) index instead of PC1 of the zonal-mean wind (section 6b). The reason for the difference between the AM and PC1 is that the vertical EP flux is symmetric about the wind anomalies in the Atlantic (which is emphasized by the AM) and asymmetric in the Pacific. During the high index, synoptic eddy activity in the Pacific is enhanced north of 40° while during the low index there is no corresponding enhancement south of 40° (not shown). Since the low index corresponds to a stronger Pacific jet (see Figs. 2a and 3a), this synoptic eddy response to PC1 seems consistent with observations of the midwinter suppression of wave activity in the Pacific (Nakamura 1992). Nakamura (1992) found that a stronger-than-normal Pacific jet does not lead to a stronger storm track. The fact that 1) the synoptic eddies are most important for the positive feedback and 2) the synoptic response to the wind anomalies involves changes in the wave source on both sides of the wind node in the Atlantic, but only on the poleward side in the Pacific, might make the eddy–zonal flow feedback significantly stronger in the Atlantic. This might explain the dominance of the Atlantic sector in AM variability. A similar effect seems even more pronounced in the SH winter where the strongest winds are in the subtropical jet over Australia yet this jet has relatively weak eddy activity and little direct role in the variability associated

with the southern AM. Thus it appears that the Pacific jet in the NH winter might be in a transition regime between a midlatitude eddy-driven jet to a subtropical jet whose variability is determined more by events in the Tropics.

Recently, there has been much interest on the possible effect of stratospheric variability on the tropospheric annular mode and the mechanisms involved in this connection (see Hartmann et al. 2000; Baldwin and Dunkerton 2001; Thompson et al. 2002). Of the feedbacks present in this paper, the quasi-stationary wave feedback, which depends on the refractive index near the tropopause, seems the most likely mechanism for this stratosphere–troposphere connection. A stronger polar night jet directly above the tropopause decreases $[u]_{zz}$, which is consistent with a decrease in the refractive index. This decrease in the refractive index implies stronger momentum fluxes into the high latitudes by the planetary waves. The possibility of stratospheric variability affecting the troposphere is also supported by Boville (1984) who showed the tropospheric response to changes in the stratosphere in a GCM. In fact, the effect of a stronger polar night jet on the tropospheric planetary waves (see his Figs. 9 and 11) is strikingly similar to the observed response to the annular mode (Fig. 12c). Moreover, the GCM run with a stronger polar night jet shows a pronounced decrease in the index of refraction poleward of 60°N in the upper troposphere (Boville 1984, his Fig. 10) compared to the control run. This is precisely the same location of the refractive index anomaly associated with the observed annular mode. Recent work by Polvani and Kushner (2002) shows that a strong tropospheric response to stratospheric forcing in a GCM does not require zonal asymmetries in the climate. This same argument might also apply in a symmetric GCM except that the refractive index for traveling waves would be used. Further work is required to test this idea and to determine whether the change in the refractive index plays a major role in the tropospheric response to stratospheric variability.

Acknowledgments. We would like to thank Jeff Yin for sharing his GCM simulations, which were helpful in developing our ideas on the stationary waves. We would also like to thank Isaac Held and an anonymous reviewer for their helpful comments and suggestions. Thanks also to the Climate Diagnostics Center for making the NCEP reanalysis data freely available online. This research was funded by the Climate Dynamics Program of the National Science Foundation under Grant ATM-9313383.

APPENDIX

Feedback Calculations

The feedback constants b_1 and b_2 are determined as in LH01. We define $\hat{z}_1$ and $\hat{m}_1$ to be z_1 and m_1 with the reduced feedback (i.e., b_1 reduced to b_2). Thus,

$$\frac{dz_1}{dt} = m_1 - \frac{z_1}{\tau} \tag{A1}$$

$$\frac{d\hat{z}_1}{dt} = \hat{m}_1 - \frac{\hat{z}_1}{\tau} \tag{A2}$$

$$\hat{m}_1 = \tilde{m}_1 + b_2\hat{z}_1, \tag{A3}$$

where $\tilde{m}_1$ is random eddy variability with no memory. Substituting (3) in (A3) we get

$$m_1 = \hat{m}_1 + b_1 z_1 - b_2\hat{z}_1. \tag{A4}$$

Taking the Fourier transform of (A1), (A2), and (A4), we get

$$M_1 = \left(\frac{1}{\tau} + i\omega\right)Z_1 \tag{A5}$$

$$\hat{M}_1 = \left(\frac{1}{\tau} + i\omega\right)\hat{Z}_1 \tag{A6}$$

$$M_1 = \hat{M}_1 + b_1 Z_1 - b_2\hat{Z}_1, \tag{A7}$$

where capital letters denote the Fourier transform of the corresponding lowercase variable. Equations (A5), (A6), and (A7) can be simply arranged to get

$$\frac{M_1}{\hat{M}_1} = \frac{Z_1}{\hat{Z}_1} \tag{A8}$$

$$\hat{Z}_1 = \frac{\sigma_1^{-1} + i\omega}{\sigma_2^{-1} + i\omega}Z_1 \tag{A9}$$

$$\hat{M}_1 = \frac{\sigma_1^{-1} + i\omega}{\sigma_2^{-1} + i\omega}M_1, \tag{A10}$$

where σ_j is defined by

$$\sigma_j^{-1} = \tau^{-1} - b_j. \tag{A11}$$

Equations (A8), (A9), and (A10) are the same form as (C4), (C5), and (C6) in LH01. Therefore, we can use the results in appendix C of LH01 with the following substitutions:

$$\tau \to \sigma_2 \tag{A12}$$

$$\sigma \to \sigma_1 \tag{A13}$$

$$b \to b_1 - b_2 \tag{A14}$$

$$\tilde{z} \to \hat{z}_1 \tag{A15}$$

$$\tilde{m} \to \hat{m}_1. \tag{A16}$$

REFERENCES

Akahori, K., and S. Yoden, 1997: Zonal flow vacillation and bimodality of baroclinic eddy life cycles in a simple global circulation model. *J. Atmos. Sci.*, **54,** 2349–2361.

Ambaum, M. H. P., B. J. Hoskins, and D. B. Stephenson, 2001: Arctic Oscillation or North Atlantic Oscillation? *J. Climate,* **14,** 3495–3507.

Baldwin, M. P., and T. J. Dunkerton, 2001: Stratospheric harbingers of anomalous weather regimes. *Science,* **294,** 581–584.

Boville, B. A., 1984: The influence of the polar night jet on the tropospheric circulation in a GCM. *J. Atmos. Sci.,* **41,** 1132–1142.

Chen, P., and W. A. Robinson, 1992: Propagation of planetary waves between the troposphere and stratosphere. *J. Atmos. Sci.,* **49,** 2533–2545.

DeWeaver, E., and S. Nigam, 2000a: Do stationary waves drive the zonal-mean jet anomalies of the northern winter? *J. Climate,* **13,** 2160–2176.

——, and ——, 2000b: Zonal-eddy dynamics of the North Atlantic Oscillation. *J. Climate,* **13,** 3893–3914.

Eady, E. T., 1949: Long waves and cyclone waves. *Tellus,* **1,** 35–52.

Edmon, H. J., B. J. Hoskins, and M. E. McIntyre, 1980: Eliassen–Palm cross sections for the troposphere. *J. Atmos. Sci.,* **37,** 2600–2616.

Feldstein, S., 1998: An observational study of the intraseasonal poleward propagation of zonal mean flow anomalies. *J. Atmos. Sci.,* **55,** 2516–2529.

——, and S. Lee, 1996: Mechanisms of zonal index variability in an aquaplanet GCM. *J. Atmos. Sci.,* **53,** 3541–3555.

——, and ——, 1998: Is the atmospheric zonal index driven by an eddy feedback? *J. Atmos. Sci.,* **55,** 3077–3086.

Hamming, R. W., 1989: *Digital Filters.* Prentice Hall, 284 pp.

Hartmann, D. L., 1995: A PV view of zonal flow vacillation. *J. Atmos. Sci.,* **52,** 2561–2676.

——, and F. Lo, 1998: Wave-driven zonal flow vacillation in the Southern Hemisphere. *J. Atmos. Sci.,* **55,** 1303–1315.

——, J. M. Wallace, V. Limpasuvan, D. W. J. Thompson, and J. R. Holton, 2000: Can ozone depletion and global warming interact to produce rapid climate change? *Proc. Natl. Acad. Sci.,* **97,** 1412–1417.

Held, I. M., 1983: Stationary and quasi-stationary eddies in the extratropical troposphere: Theory. *Large Scale Dynamical Processes in the Atmosphere,* R. P. Pearce and B. J. Hoskins, Eds., Academic Press, 127–168.

——, and M. J. Suarez, 1994: A proposal for the intercomparison of the dynamical cores of atmospheric general circulation models. *Bull. Amer. Meteor. Soc.,* **75,** 1825–1830.

——, R. L. Panetta, and R. T. Pierrehumbert, 1985: Stationary external Rossby waves in vertical shear. *J. Atmos. Sci.,* **42,** 865–883.

Hoerling, M. P., M. Ting, and A. Kumar, 1995: Zonal flow–stationary wave relationship during El Nino: Implications for seasonal forecasting. *J. Climate,* **8,** 1838–1852.

Hoskins, B. J., and T. Ambrizzi, 1993: Rossby wave propagation on a realistic longitudinally varying flow. *J. Atmos. Sci.,* **50,** 1661–1671.

Hu, Y., and K. K. Tung, 2002: Interannual and decadal variations of planetary wave activity, stratospheric cooling, and Northern Hemisphere annular mode. *J. Climate,* **15,** 1659–1673.

James, I. N., and P. M. James, 1992: Spatial structure of ultra-low-frequency variability of the flow in a simple atmospheric circulation model. *Quart. J. Roy. Meteor. Soc.,* **118,** 1211–1233.

Kalnay, E., and Coauthors, 1996: The NCEP/NCAR 40-Year Reanalysis Project. *Bull. Amer. Meteor. Soc.,* **77,** 437–471.

Karoly, D. J., 1990: The role of transient eddies in the low-frequency zonal variations in the Southern Hemisphere circulation. *Tellus,* **42A,** 41–50.

Kidson, J. W., 1988: Indices of the Southern Hemisphere zonal wind. *J. Climate,* **1,** 183–194.

Kimoto, M., F. F. Jin, M. Watanabe, and N. Yasutomi, 2001: Zonal-eddy coupling and a neutral mode theory for the Arctic Oscillation. *Geophys. Res. Lett.,* **28,** 737–740.

Lee, S., and S. B. Feldstein, 1996: Mechanisms of zonal index evolution in a two-layer model. *J. Atmos. Sci.,* **53,** 2232–2246.

Limpasuvan, V., and D. L. Hartmann, 1999: Eddies and the annular modes of climate variability. *Geophys. Res. Lett.,* **26,** 3133–3136.

——, and ——, 2000: Wave-maintained annular modes of climate variability. *J. Climate,* **13,** 4414–4429.

Lorenz, D. J., and D. L. Hartmann, 2001: Eddy-zonal flow feedback in the Southern Hemisphere. *J. Atmos. Sci.,* **58,** 3312–3327.

Madden, R. A., and P. Speth, 1995: Estimates of atmospheric angular momentum, friction, mountain torques during 1987–1988. *J. Atmos. Sci.,* **52,** 3681–3694.

Matsuno, T., 1970: Vertical propagation of stationary planetary waves in the winter Northern Hemisphere. *J. Atmos. Sci.,* **27,** 871–883.

Nakamura, H., 1992: Midwinter suppression of baroclinic wave activity in the Pacific. *J. Atmos. Sci.,* **49,** 1629–1642.

North, G. R., F. J. Moeng, T. L. Bell, and R. F. Cahalan, 1982a: The latitude dependence of the variance of zonally averaged quantities. *Mon. Wea. Rev.,* **110,** 319–326.

——, T. L. Bell, R. F. Cahalan, and F. J. Moeng, 1982b: Sampling errors in the estimation of empirical orthogonal functions. *Mon. Wea. Rev.,* **110,** 699–706.

Polvani, L. M., and P. J. Kushner, 2002: Tropospheric response to stratospheric perturbations in a relatively simple general circulation model. *Geophys. Res. Lett.,* **29** (7), doi:10.1029/2001GL014284.

Robinson, W. A., 1991: The dynamics of the zonal index in a simple model of the atmosphere. *Tellus,* **43A,** 295–305.

——, 1994: Eddy feedbacks on the zonal index and eddy–zonal flow interactions induced by zonal flow transience. *J. Atmos. Sci.,* **51,** 2553–2562.

——, 1996: Does eddy feedback sustain variability in the zonal index? *J. Atmos. Sci.,* **53,** 3556–3569.

——, 2000: A baroclinic mechanism for the eddy feedback on the zonal index. *J. Atmos. Sci.,* **57,** 415–422.

Thompson, D. W. J., and J. M. Wallace, 2000: Annular modes in the extratropical circulation. Part I: Month-to-month variability. *J. Climate,* **13,** 1000–1016.

——, M. P. Baldwin, and J. M. Wallace, 2002: Stratospheric connection to Northern Hemisphere wintertime weather: Implications for prediction. *J. Climate,* **15,** 1421–1428.

Wolter, K., and M. S. Timlin, 1993: Monitoring ENSO in COADS with a seasonally adjusted principal component index. *Proc. 17th Climate Diagnostics Workshop,* Norman, OK, NOAA/NMC/CAC, 52–57.

——, and ——, 1998: Measuring the strength of ENSO—How does 1997/98 rank? *Weather,* **53,** 315–324.

Yang, G. Y., and B. J. Hoskins, 1996: Propagation of Rossby waves of nonzero frequency. *J. Atmos. Sci.,* **53,** 2365–2378.

Yu, J.-Y., and D. L. Hartmann, 1993: Zonal flow vacillation and eddy forcing in a simple GCM of the atmosphere. *J. Atmos. Sci.,* **50,** 3244–3259.